Computers & Geosciences 44 (2012) 100–108

Contents lists available at SciVerse ScienceDirect

Computers & Geosciences

journal homepage: www.elsevier.com/locate/cageo

A grid implementation of the SLUTH algorithm for visualising the depth and structural index of magnetic sources

Richard S. Smith [a,*], Jeffrey B. Thurston [b], Ahmed Salem [c,d,e], Alan B. Reid [f]

[a] Department of Earth Sciences, Laurentian University, 935 Ramsey Lake Road, Sudbury, ON P3E 2C6, Canada
[b] 3628 7A St SW, Calgary, AB T2T 2Y5, Canada
[c] GETECH, Kitson House, Elmete Hall, Elmete Lane, Leeds, LS8 2LJ, UK
[d] University of Leeds, UK
[e] Nuclear Materials Authority, PO Box 530 Maadi,Cairo, Egypt
[f] School of Earth & Environment, University of Leeds, and Reid Geophysics Ltd., 7 Keymer House, Michel Grove, Eastbourne, BN21 1JZ, UK

ARTICLE INFO

Article history:
Received 10 November 2011
Received in revised form
1 March 2012
Accepted 3 March 2012
Available online 16 March 2012

Keywords:
Automatic
Interpretation
Image
Basement
Structure

ABSTRACT

The SLUTH method requires first-order derivatives at two or more different heights above the ground and can estimate the location and depth of source bodies from magnetic data. Results of this method are independent of a specific model type and can be used to estimate the most appropriate model (structural index). This paper presents a grid implementation of the SLUTH method to visualise both depth and structural index from magnetic anomaly data. The implementation uses the Geosoft GX programming language. The method has been tested using theoretical magnetic gridded data and two methods have been used for estimating depth; the estimate from the width of the imaged feature gives an underestimate and the estimate from the rate of fall off of the field with height gives an overestimate. The practical utility of the algorithm is demonstrated using field data from the Saskatoon area of Canada.

1. Introduction

In recent years a number of methods have been introduced for extracting source parameters from magnetic data. The commonly used methods are Euler deconvolution (Ruddock et al., 1966; Thompson, 1982; Reid et al., 1990), the Naudy method (Naudy, 1971), Werner deconvolution (Hartman et al., 1971), the analytic signal method (Nabighian, 1972; Roest et al., 1992) and use of the local wavenumber (Thurston and Smith, 1997; Keating, 2009). In recent years the use of "similarity transforms" has also been proposed for interpreting magnetic data (Stavrev et al., 2009; Gerovska et al., 2010). Most of the methods use spatial derivatives of the magnetic field and generally require some assumption about the shape of the causative body. Methods that relax assumptions about the shape of the causative body often require higher-order derivatives (Smith et al., 1998; Thurston et al., 2002; Salem et al., 2005; Salem et al., 2008) which can be problematic as the calculation of the higher-order derivative can amplify noise in the data.

A patent application in Ruddock et al. (1966) suggested using the magnetic field measured at two different heights to allow the calculation of a vertical derivative. In recent years a number of magnetic interpretation techniques have been introduced that also use data at multiple heights. Application of these methods, to surveys acquired at a single sensor elevation, requires numerical continuation to a greater height (Dean, 1958). Like introducing higher-order derivatives into the methods, introducing continuation also provides a means for constraining the source geometry. However, unlike gradient computation, upward continuation does not introduce instability due to amplification of high-frequency noise (Lahti and Karinen, 2010). Techniques which use wavelets (Moreau et al., 1997; Hornby et al., 1999; Sailhac et al., 2000; Vallee et al., 2004; Fedi, 2007; Cella et al., 2009; Sailhac et al., 2009) use upward continuation implicitly or explicitly and are also able to estimate the causative structure.

The calculation of higher-order derivatives requires special attention (Pasteka et al., 2009); this is particularly so for gridded data, which is generally derived from profile data by sub-sampling and interpolation. Thus, a group of workers have proposed calculating the derivatives from profile data (Salem and Smith, 2005; Smith and Salem, 2005; Smith et al., 2005) as the lateral spacing of the samples is finer and the signal fidelity is higher on profile data than it is on gridded data. However, displaying these profile results on an image is not straightforward.

* Corresponding author. Tel.: +1 705 675 1151.
E-mail addresses: RSSmith@laurentian.ca (R.S. Smith), jbthurston@gmail.com (J.B. Thurston), Ahmed.Salem@getech.com (A. Salem), alan@reid-geophys.co.uk (A.B. Reid).

0098-3004/$ - see front matter © 2012 Elsevier Ltd. All rights reserved.
http://dx.doi.org/10.1016/j.cageo.2012.03.004

The SLUTH method proposed by Thurston and Smith (2007) and implemented by Ulla et al. (2010) uses upward-continued data and only requires first-order derivatives, so it is more robust in the presence of noise than the methods that require higher-order derivatives. The Ulla et al. implementation is tailored specifically to profile data, but the SLUTH method could also be implemented on grids as first-order derivatives can normally be calculated fairly well on gridded data. The advantage of grid implementation is the ability to display the results in a manner that can be easily visualised and incorporated with other geological and geophysical maps. To this end, we have chosen to display the results using the same display approach as the tilt–depth method of Salem et al. (2007, 2010). The resulting images can be obtained without reduction to the pole or the calculation of higher-order derivatives, nor are they also only valid for vertical contacts; all of which are restrictions of the tilt–depth method.

We have chosen to implement SLUTH in the Geosoft GX language (or API), allowing all users of the Geosoft montaj geophysical software to run the method. The input to the algorithm is gridded magnetic data on two height levels (the acquisition height and an upward continued height) plus the associated vertical and horizontal derivatives. Geosoft montaj has a GX tool (mapmap1) for upward continuing the data and calculating all the required spatial derivatives. The GX is available from http://www.iamg.org. The source code is also available for those who would like to translate the code and implement the algorithm in another environment.

2. The method

The SLUTH method (Thurston and Smith, 2007, Ulla et al., 2010) uses the quantity m which is the negative of the ratio of the horizontal to the vertical derivatives

$$m = -\frac{\mathrm{d}T/\mathrm{d}x}{\mathrm{d}T/\mathrm{d}z} \quad (1)$$

where T is the total magnetic field, z is the vertical direction, and x is the horizontal direction. The quantity m is the inverse of the ratio used in the tilt angle quantity proposed by Miller and Singh (1994) and utilised by Salem et al. (2007) in their tilt–depth method. Hence small values of the tilt angle correspond to large values of m. The procedure requires that the magnetic field and its horizontal and vertical derivatives be known on one or more datums (or heights) at or above the earth's surface. Fig. 1 shows an aeromagnetic-survey aircraft and the datum along which the measurements are acquired. The derivatives could be measured or calculated. Also shown in Fig. 1 is a second (higher) level, in this case called the upward continued datum, as the measurements at this level can be calculated by upward continuation (Dean, 1958) from the values on the lower measurement datum. However, the field values and the derivatives could also be measured on this datum. The quantity m is calculated at all locations on the measurement and upward continued datums, and then similar values of m are sought on the upper and lower datums. Fig. 1 shows the locations of three pairs of identical values on the lower and upper datums. The first pair consists of a value m_{al} on the lower datum that is equal to the value m_{au} on the upper datum. Joining these two locations creates a ray. Similarly, rays can be drawn through the pairs (m_{bl}, m_{bu}) and (m_{cl}, m_{cu}). For homogeneous sources, these rays intersect at the location of the magnetic source body (Thurston and Smith, 2007). Note that this procedure can be applied for more than three pairs and more than two datums. The angle that the ray makes with a vertical line is important. Fig. 1 shows the angle from the vertical θ_c for the ray associated with the pair (m_{cl}, m_{cu}). If the angle θ_c is zero, then the ray is directly above the source of the magnetic anomaly. Thurston and Smith (2007); Ulla et al. (2010) assumed that the sources were 2D and perpendicular to the flight lines. This means that the rays drawn on Fig. 1 are actually planes that extend in and out of the page.

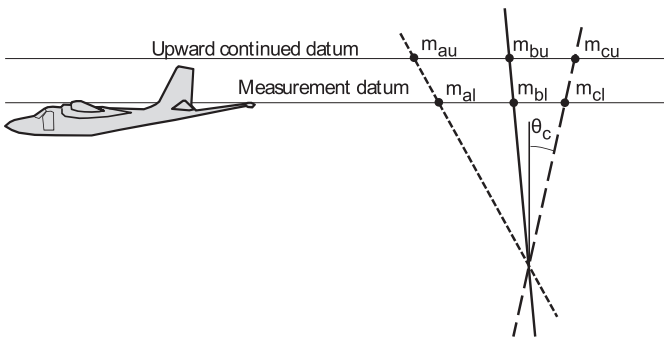

Fig. 1. The basic principle of the SLUTH method. The field is measured on a measurement datum and upward continued to a higher datum. The horizontal and vertical spatial derivatives are calculated on both datums and the ratio used to calculate the m values. Rays are drawn along lines joining similar m values on the two datums and these rays converge at the source location. The angle of the ray from the vertical is given by the angle θ.

2.1. Grid implementation

Fig. 2 shows an oblique 3D view of part of the measurement datum and part of the upward continued datum. Eighteen grid points are shown on each datum, but the grid will extend outward in all four directions. The dark point on the measurement datum shows a specific point and the dashed line joins this point to the corresponding point directly above on the upward continued datum. Surrounding this central point are eight nearby points, four in the cardinal directions and four on diagonal or inter-cardinal directions. In the upper datum surface, solid lines have been drawn in the cardinal directions joining these nine points.

The value of m is calculated at the central point on the lower datum, and then the locations where similar m value occurs on the upper datum are estimated. This can be done using a variety of approaches, but we have chosen to use linear interpolation between the points along the solid lines. Fig. 3 shows four dots on the upper datum that have similar m values to the central value on the lower datum. These four points define a line which we call the strike line. The strike line and the lower central point together form a ray plane, shown on Fig. 3 as a shaded plane. In some cases there may only be one, two or three location on the upper datum where the m values are the same as the central m value on the lower datum. In cases when there are more than two points, the degree of misfit from a straight line could be used as a measure of

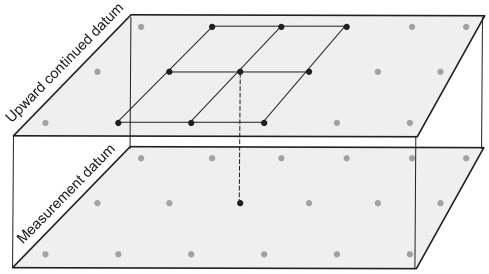

Fig. 2. Oblique 3D view of the upper and lower datums. The dotted line joins a grid point on the upper datum directly above a point on the lower datum. There are nine points in a window on the upper datum (including the central point).

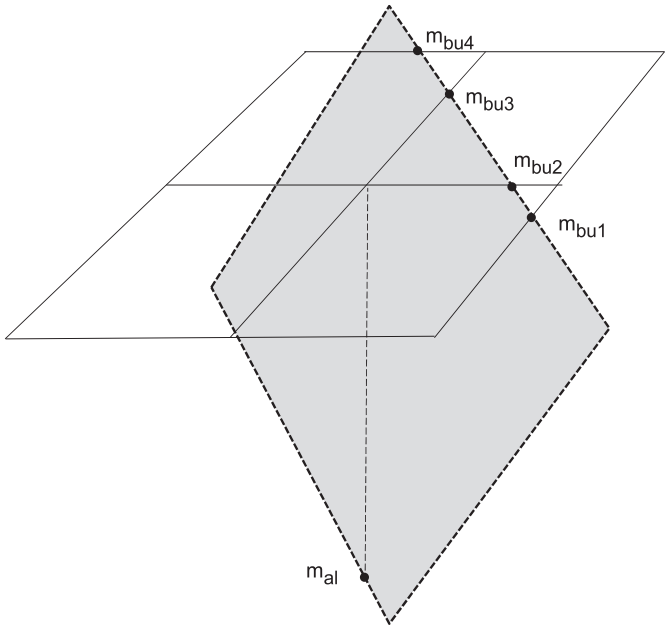

Fig. 3. The m value at the central point on the lower datum is m_{al}. Similar values are sought on the lines joining the 9 points on the upper datum. In this case, there are four points obtained, forming a straight horizontal line. This line is the strike direction of the ray plane shown in grey, which is the extension to 3D of the rays drawn on Fig. 1. The source location is at greater depth on the ray plane, where this ray plane intersects with another ray plane.

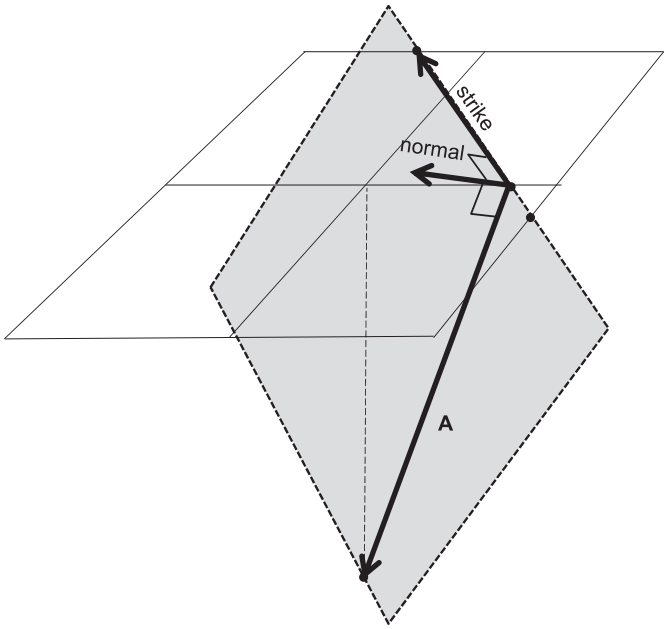

Fig. 4. The normal to the ray plane can be obtained as the vector normal to any two non-parallel vectors in the ray plane. In this case, the non-parallel vectors are the strike vector and the vector **A** from a point on the strike line to the central point on the lower datum.

the noise in the data or of the quality of fit and hence the validity of the assumption that the model is a 2D homogeneous source. If the model is 2D, the direction of the horizontal gradient vector should be perpendicular to the strike direction. The deviation of this angle from 90 degrees could also be used as a measure of when the model is not 2D.

The strike line is horizontal and thus it defines the strike direction of the 2D structure. The cross product of this strike direction and any other non-horizontal vector in the ray plane gives the normal to the plane. One choice for the non-horizontal vector is a vector A that goes from the central point on the lower datum to a point on the strike line on the upward continued datum. Fig. 4 shows these two vectors and the cross product that is normal to the plane. A vector in the dip direction is the cross product of the strike vector with the normal vector (Fig. 5). To ensure that the dip vector is pointing down, the z component should be pointing down. If not, multiply the dip vector by negative one. The angle of the ray plane from the vertical can be obtained by calculating the dot product of the dip vector with the vertical vector.

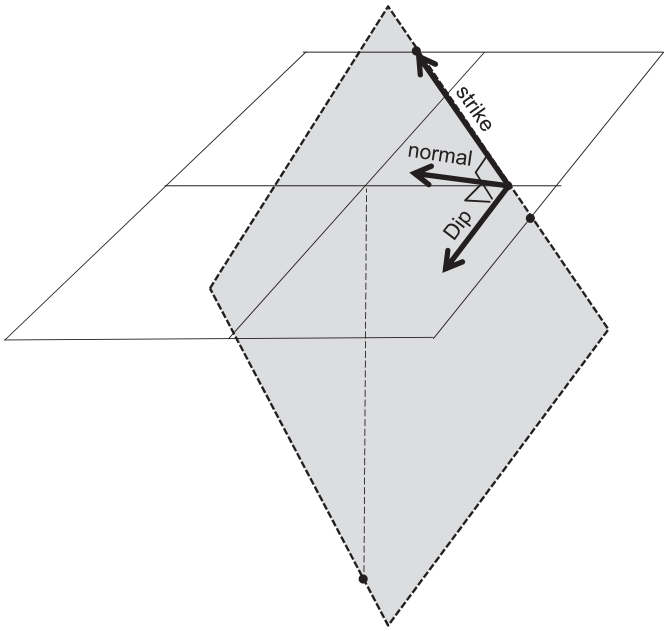

Fig. 5. The dip vector is perpendicular to the normal vector and the strike vector.

2.2. Depth to source

It is possible to estimate the distance r from the source to the central point on the lower measurement datum. This is obtained using the relations for homogeneous functions.

$$T(cr) = c^n T(r) \tag{2}$$

$$\frac{dT}{dz}(cr) = c^{n-1}\frac{dT}{dz}(r) \tag{3}$$

or,

$$\frac{dT}{dx}(cr) = c^{n-1}\frac{dT}{dx}(r) \tag{4}$$

where r is a distance from the point that defines the magnetic source and c is a scale factor. The value of T (or the derivatives) at r are the known values at the central point on the lower datum. The values of T (and the derivatives) on the strike line on the upper datum can be calculated by interpolation from the known values at the grid nodes. These values are at a distance cr from the source. From these values, the scale factor c can be estimated from

$$c = \frac{T(cr)/T(r)}{(dT/dx)(cr)/(dT/dx)(r)} \tag{5}$$

and/or

$$c = \frac{T(cr)/T(r)}{(dT/dz)(cr)/(dT/dz)(r)} \tag{6}$$

In Eqs. (4)–(6), the x derivative is actually the total horizontal derivative $\sqrt{(dT/dx)^2+(dT/dy)^2}$. The distance from the point on the lower datum up the dip vector to the point where it intersects with the upper datum (Fig. 6) is Δr. From the definition of Δr and c, we have $cr=r+\Delta r$, so

$$r=\frac{\Delta r}{c-1} \tag{7}$$

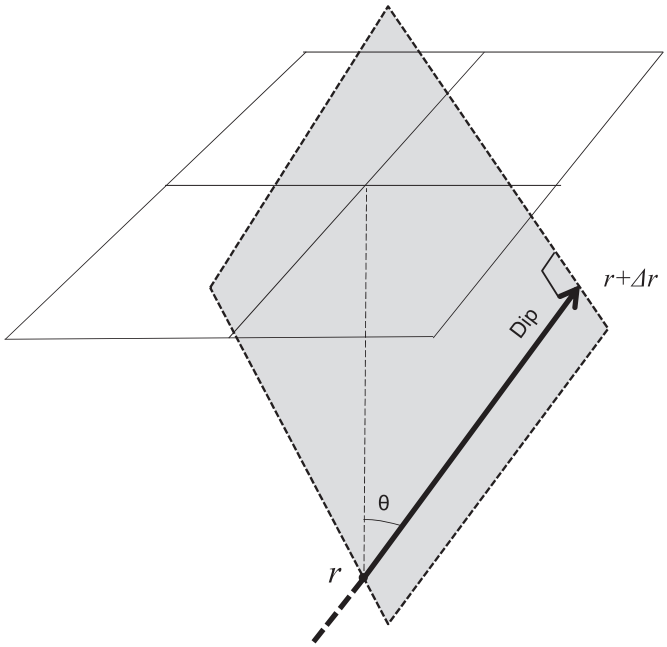

Fig. 6. The distance Δr from the central point on the lower datum to the closest point on the strike line on the upper datum is along the dip vector. If the distance from the source to the central point on the lower datum is r, then the distance to the strike line is $r+\Delta r$. The angle of the ray plane from the vertical is θ.

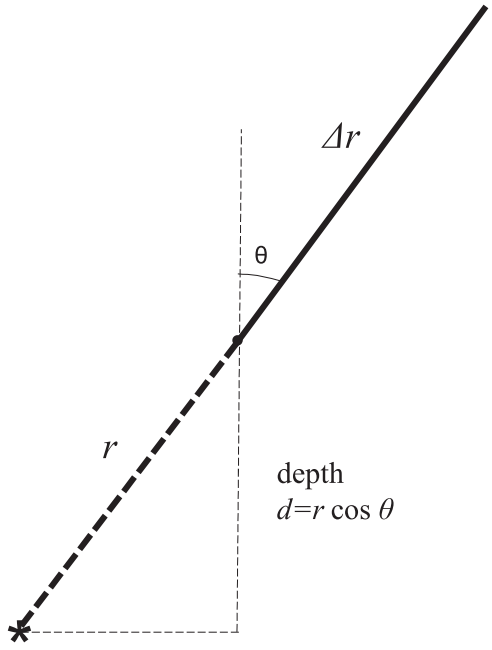

Fig. 7. The distance from the source location (*) to the central point on the lower datum is r. The depth to the source d from the lower datum is $r\cos\theta$.

The depth d to the source from the lower measurement datum is (Fig. 7)

$$d=r\cos\theta \tag{8}$$

where θ is the angle from the vertical to the ray plane (Figs. 6 and 7).

2.3. Structural index

Using Eqs. (3) or (4), it is possible to calculate the structural index or degree of inhomogeneity n. The value of n at each grid point can be calculated from Eqs. (2), (3) or (4). For example

$$n=\ln\left(\frac{T(cr)}{T(r)}\right)/\ln(c) \tag{9}$$

or

$$n=\frac{\ln((dT(cr)/dz)/(dT(r)/dz))}{\ln(c)}+1 \tag{10}$$

2.4. Algorithm

The SLUTH grid implementation requires that the field and the spatial derivatives be known on the upper and lower measurement datums. These can be calculated by upward continuation of the field from the lower datum to the upper datum. On each datum the spatial derivatives are calculated from the total field. We found that calculating the vertical derivative in the frequency domain and horizontal derivatives in the space domain can lead to inconsistent results because the characteristic points on the curve were shifted relative to where they should be. We found that good results were obtained when all the derivatives and the upward continuation are calculated in the frequency domain. This can be done in the Geosoft Oasis montaj software package using the "magmap1" GX. Whenever frequency-domain operations are performed on grids that will be added/subtracted or otherwise operated on. the best results will be obtained when the same padding, extrapolation and low pass filtering are applied to all the grids.

The following procedure is then applied at each grid point:

1) Calculate the m values on the lower and upper datums
2) Find the m value at the central point on the lower measurement datum.
3) Look for locations of similar values on the upper datum and fit a straight line to these upper datum locations to determine the strike direction of the ray plane. The misfit from the line-fitting will provide an estimate of the error. When there are three or more locations, there will be three or more strikes that we can calculate and our simple way of estimating the error is to calculate the standard deviation of these strikes. More sophisticated ways are possible.
4) Calculate the normal to the ray plane, the dip vector and the angle of the dip vector from the vertical, θ.
5) Estimate c using the values of T and the derivatives at the lower central point and the values on the upper datum.
6) Estimate Δr and then the distance r of the lower grid point to the source and then the corresponding depth d.
7) Estimate the structural index.

This procedure has been implemented as a Geosoft GX called gridsluth that can be run within the Oasis Montaj geophysical data processing software. The output from the GX are grids of the strike in degrees from north, the standard deviation of the strike, the structural index, and the depth. The latter are output in grid cell units, so must be converted to dimensioned units by multiplying by the grid cell spacing in the appropriate dimensioned units.

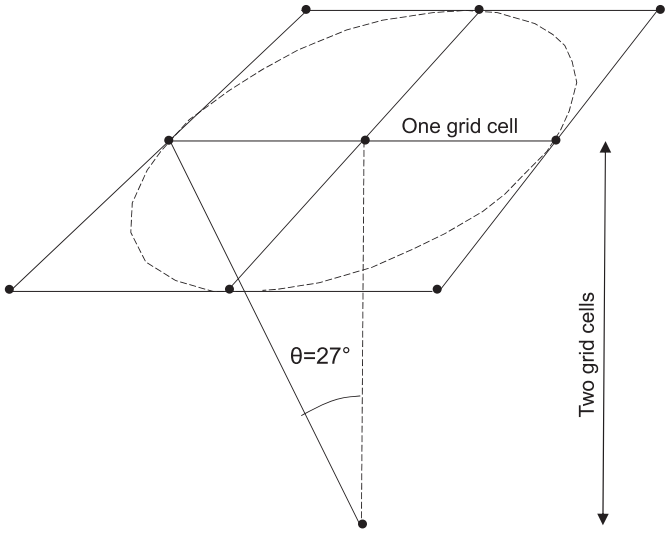

Fig. 8. When the upward continued datum is two grid cells above the measurement datum, ray planes with angles less than 27 degrees (inside the dotted circle) can be determined reliably. Greater angles can be determined when the strike directions are close to 45 and 135 degrees.

2.5. Display of results

The derived quantities (for example, depth, fit, structural index, strike, angle of ray plane from vertical) can be estimated at all grid points. However, it only makes sense to display the results when the grid cell is judged to be close to a magnetic source. The grid cells are close to the magnetic source when the ray plane is close to vertical. Our approach is to display the results using a method similar to that proposed by Salem et al. (2007), who made the map dark where the tilt angle was less than 45 degrees, creating a zone on the map twice as wide as the depth to the source. In our implementation, the data on the lower measurement datum will be upward continued 1 or 2 grid cell spacings. Fig. 8 shows the case when it is two grid cell spacings, when a dip angle of 27 degrees or less ensures that the ray plane intersects the upper datum between the central point and the nearest grid point (s). The grid locations where the ray plane is less than 27 degrees will be coloured. This will create a zone with a width equal to the depth to the source below the measurement datum. The colour of the zone could be set according to the numerical value of any of the derived quantities (for example, structural index or standard deviation of the strike). It is also possible to colour the image according to the depth and strike and dip angles; however, this information will be somewhat redundant as the same information will already be evident from the shape of the coloured areas. One advantage of displaying this redundant information is that the consistency of the parameters will give an indication of how good the model is and how well the method is working in this area.

Poor solutions will also be obtained when our assumptions are not satisfied. We have assumed that the magnetic sources are 2D and the structural indices of 2D magnetic sources range between 0 and 2. However structural index values of 3 are also valid for dipole (3D) sources (Stavrev and Reid, 2007). If the 3D sources are sufficiently deep and the spatial derivatives are adequately sampled on the grid, then there may be some information in the processed data that could be extracted so as to assist in an interpretation. So, rather than only displaying solutions with valid 2D indices between 0 and 2, we have elected to display the results for indices greater than zero and less than 3. In order to allow some margin for errors, we restrict the valid range of structural indices from -0.5 to 3.5.

3. Synthetic examples

A synthetic data set presented by Salem et al. (2008) has been used to test the grid implementation of the SLUTH method.

Fig. 9 shows the magnetic field on the lower datum. The long linear feature is a vertical thin dike at a depth of 5 km with a magnetisation of 5 A/m; the smaller body (top right) is a vertical sided prism at a depth of 3 km and a magnetisation of 0.4 A/m;

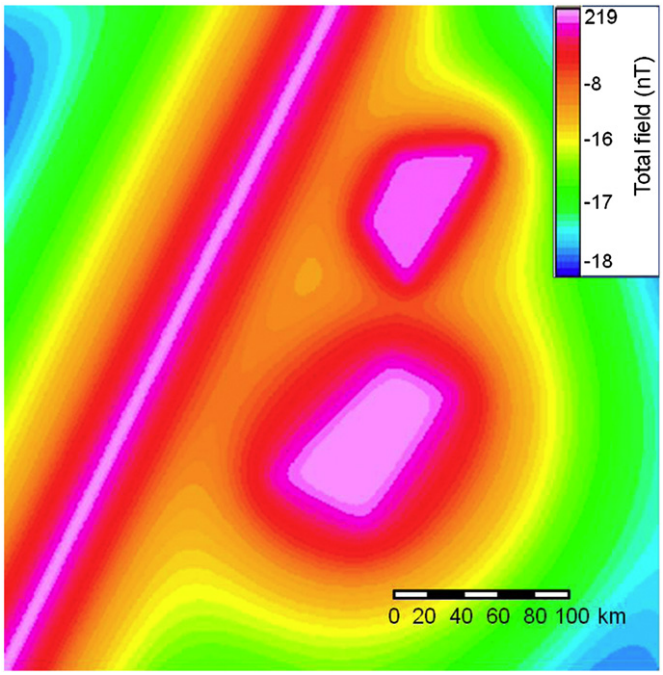

Fig. 9. The magnetic total field for a synthetic model containing a dyke buried at 5 km with a magnetisation of 5 A/m (left feature); a vertical sided prism with a magnetisation of 0.4 A/m and buried at a depth of 3 km (top right); and a larger vertical prism with a magnetisation of 0.6 A/m and a depth to top of 7 km (bottom right). The magnetisation is assumed induced by a vertical field.

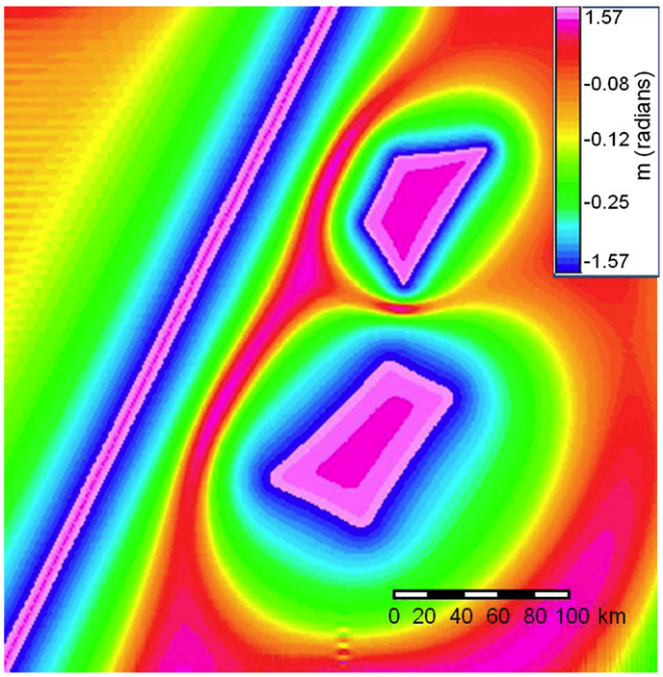

Fig. 10. The m values (where $m=-(dT/dx)/(dT/dz)$) for the synthetic data in Fig. 9.

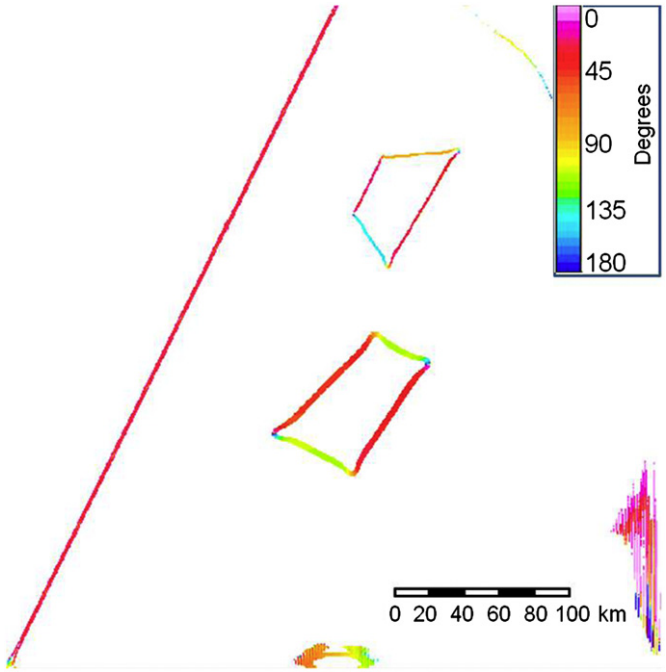

Fig. 11. The strike angle estimated from the trend defined by the *m* values on the upper datum. Zero degrees corresponds to a north–south strike, 90 degrees is an east west strike and 180 degrees is also north–south. Note the noise artifacts on the edges of the grid where the fields are small and the gradients weak.

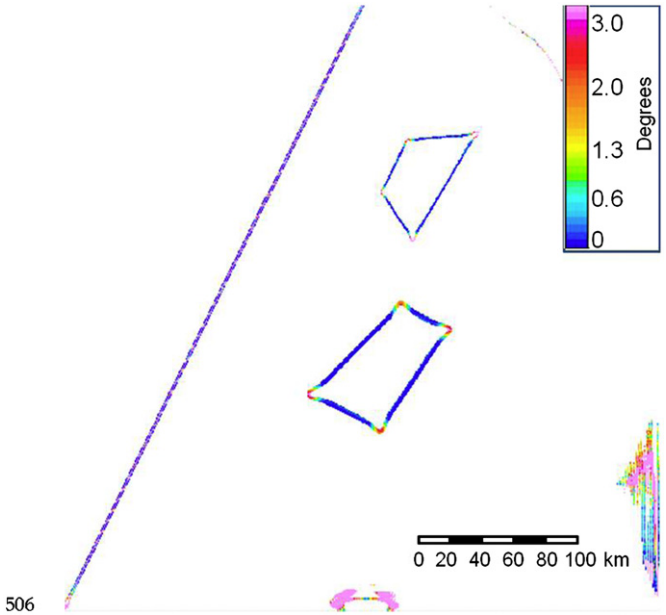

Fig. 12. The standard deviation of the strike estimates in Fig. 11. Blue values imply a good estimate of the strike, warmer colours are poorer estimates.

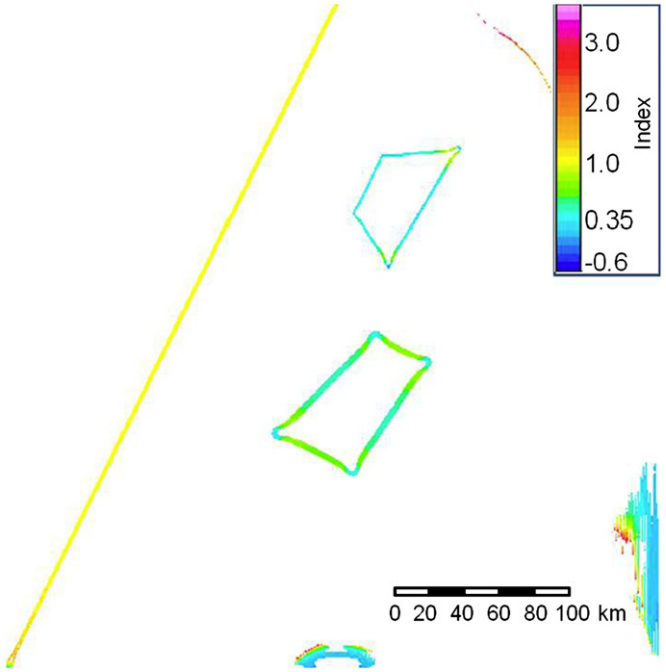

Fig. 13. The estimate of the structural index *n*.

and the larger body (bottom right) is a vertical prism with a magnetisation of 0.6 A/m and a depth to top of 7 km. The magnetisation is induced by a field inclined at 90 degrees. The *m* values on the lower datum are shown on Fig. 10, the image of the *m* values on the upper datum look very similar, but the values differ slightly. Applying the SLUTH algorithm, gives the results displayed on Figs. 11 to 14. The strike angle is shown on Fig. 11, where zero degrees corresponds to a north–south strike, 90 degrees is east west and 180 degrees is also north south. The colours correspond to the correct strike of the features on the map. The standard deviation of the strike is shown on Fig. 12. Generally the deviations are less than 0.6 degrees, except at the source-body vertices, where a poor estimate of the strike is expected as the model departs significantly from being 2D. The structural index is shown on Fig. 13. The vertical prisms are approximately 2D contacts close to the centre of each edge, so the structural index should should be close to zero and this is almost the case (the index is about 0.35), but towards the vertices, the index increases to about 0.7. The estimated index for the dike is about 1.1, which is close to the expected value of 1.0. The depth is shown on Fig. 14. The dike model has colours that indicate a depth of 5.5 km (cf 5 km), the top prism has colours corresponding to depths about 4 km (cf 3 km) in the centres of the edges and larger towards the vertices. The bottom prism has depths of 10 km or more (cf 7 km). In all cases the depths derived from Eq. (8) are overestimates; however, the depths from the width of the zone that is coloured are not overestimates. In fact, the zone associated with the top prism is actually 2.5 km wide, the width of the dike is 4.5 km and the width of the bottom prism is 6 km. There are difficulties in reading widths from the images, as Geosoft interpolates between grid values on images and it is not clear how it deals with displaying null values and grid cells next to null values. Given the above results, we should emphasise that the SLUTH grid images should be used to identify relative changes in the source parameters and not for determining the exact value. If the exact values are required, then the data should be modelled.

On Figs. 11–14 there are coloured artifacts on the edges of the images that are not associated with the three bodies. These are where the magnetic field is small and hence the gradients will be small. We should therefore expect noise artifacts such as these in areas where the magnetic field are weak or relatively flat.

4. Field examples

4.1. Saskatoon area

The grid implementation of the SLUTH method has been tested on field data collected by the GSC in the Saskatoon area of Canada

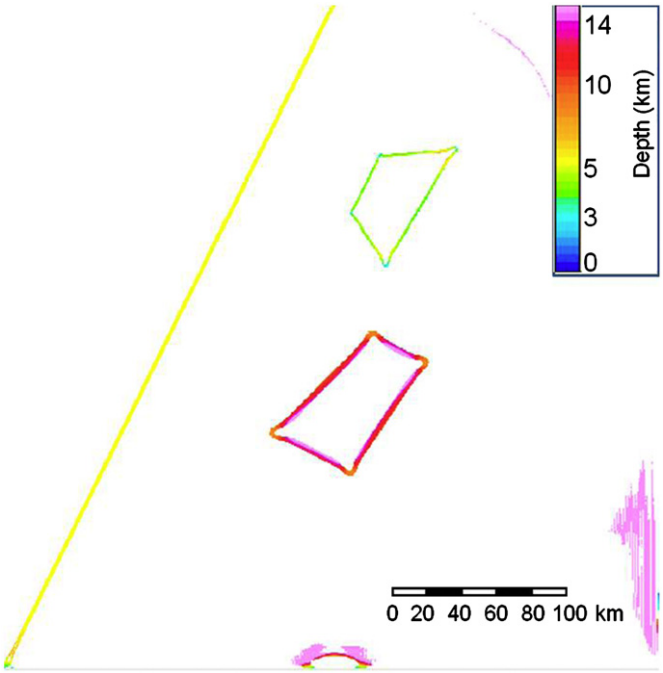

Fig. 14. The depth to the structure. The width of the coloured zone is also an indication of the depth.

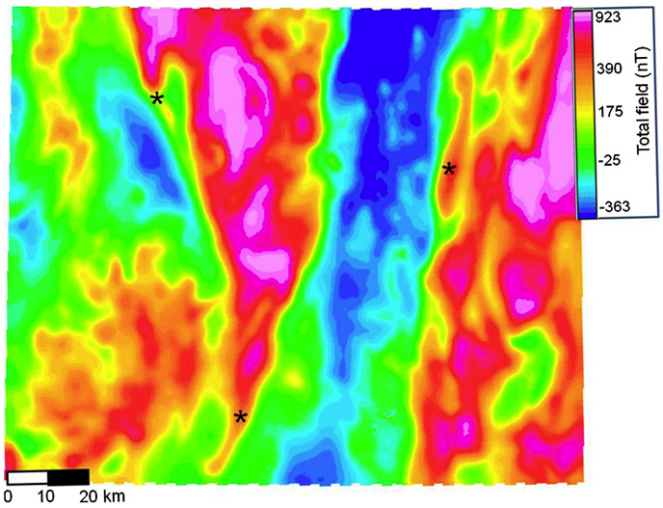

Fig. 15. Magnetic map showing the Saskatoon area. North is to the top. The area is 143 km wide and 117 km high. Three asterisks are used to indicate narrow magnetic features.

(Geological Survey of Canada, 1995). Fig. 15 shows the total magnetic field data over an area 143 km wide by 117 km high. The aircraft flight height was 150 m, the flight lines are east–west at a spacing of 800 m and the grid cell size is 200 m. A scale bar is shown at the bottom left and the colour bar is at the top right. The basement in this part of the Western Canada Sedimentary Basin is largely unexplored; however, broadly speaking, the primary non-magnetic Phanerozoic sediments in this part of southern Saskatchewan extend from surface to about 1200 m below surface in the top right to 1800 m below surface at bottom left (Saskatchewan Geological Survey, 1999). There are strong magnetic features evident in the image, a magnetic high on the eastern side of the image, a magnetic low and a wedge of high magnetic material in the centre. This wedge is widest at the north and narrows to the south. Also marked with asterisk symbols are three narrow features. These magnetic features are associated with basement rocks, probably the Proterozoic Reindeer zone, which outcrops to the north. Fig. 16 is an image of the structural index of the magnetic sources. The map is largely blue (less than 0.35), indicating that most features are contacts or faults separating one relatively wide domain from another wide domain. There are a number of structures with indices greater than 1.0. Note that these correspond to the narrower features marked with asterisks, so they could be dykes or ribbon models. The depth image (Fig. 17) shows that the principal features are 1.5 km deep or deeper, which is consistent with the depth to basement in the area. These depths are consistent with the width of the features which seem to be about 3 km wide. The zones of weak magnetic response (blue zones on Fig. 15) correspond with pink zones in Fig. 17, implying that the magnetic sources are much deeper in these areas. However, these blue zones on Fig. 15 are where the magnetic field is weak, so we should not necessarily pay too much attention to these results, as the synthetic modelling implies we might see noise artifacts in these zones. This zone could represent a basement low not identified on the geological map (Saskatchewan Geological Survey, 1999). The basement depths are interpreted to increase to the south, but this is not clearly evident in the depth image (Fig. 17). One possible explanation for this is that the

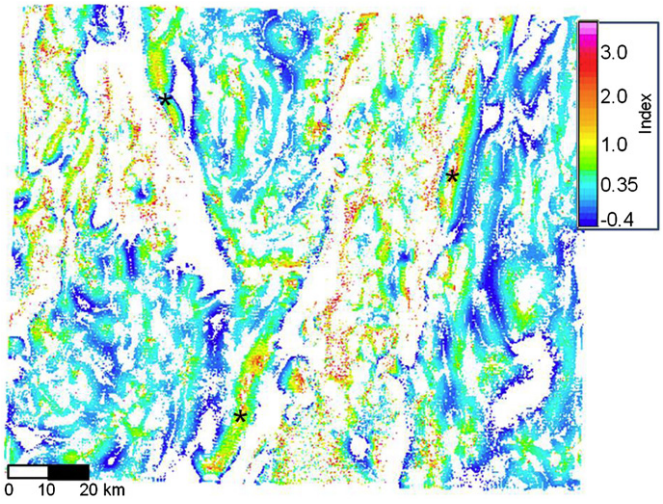

Fig. 16. The structural index map of the Saskatoon area.

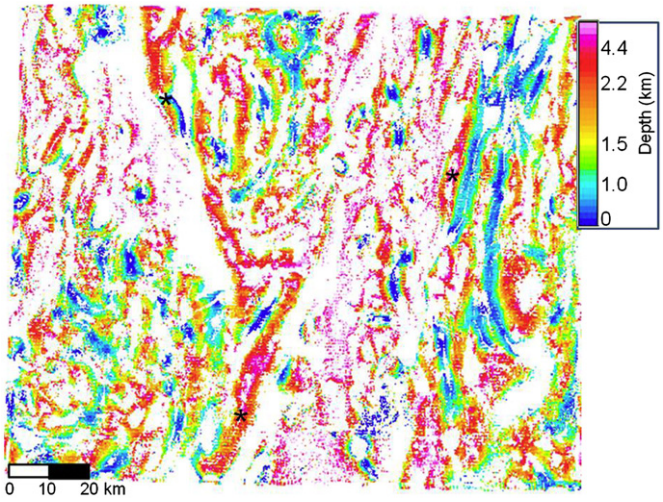

Fig. 17. The depth map of the Saskatoon area.

strongest magnetic features are coming from sources below the sediment/basement interface. Note that there are many strong features adjacent to each other in the magnetic data, so interference will be a problem when interpreting this data set.

The depth results on Fig. 17 show some artefacts aligning with the east–west flight lines. More careful gridding of the data could reduce these artefacts. Also, filtering of the resultant image could remove some of the single point features and ragged nature of the image. However, we have elected not to do this, so that the reader can see the raw unadulterated results.

An example of the type of information that can be extracted from these images can be inferred by looking at the asterisk on the upper left of the image. Above the asterisk, there is a stronger magnetic feature and below the asterisk the feature is weaker. The depth information indicates that the depths are similar, so the stronger magnetic anomaly could be due to more susceptible or thicker material to the north.

5. Discussion

The SLUTH method uses only first derivatives, so it is robust to noise compared with methods like the tilt–angle derivative method (Salem et al., 2008), which require second derivatives and upward continuation to ensure stability. The disadvantage is that the c value and hence the depth estimate derived using Eqs. 7 and 8 use the magnitude of the total field and the first derivatives. If there is interference from surrounding sources, then the magnetic field and hence the c value will be distorted and the depth estimate will also be distorted. The interference can be reduced by using higher order derivatives (which are sharper and less subject to interference), but this would involve using first- and second-order derivatives to estimate the c value and the depth. The drawback is that these higher order derivatives are noisier, making the depth estimate less reliable. Other grid implementations of the SLUTH method using similar strategies are also possible.

A detailed analysis of the robustness of the SLUTH method to interference was undertaken by Ulla et al. (2010). They showed that there was minimal interference between two vertical dykes when the two dykes were a distance apart that was more than three times the depth that the dyke was buried below the sensor.

Ulla et al. (2010) also analysed the robustness of the SLUTH method to random noise and found that reasonable estimates of the depth could be obtained when the random noise was less than 1 nT.

We have chosen to implement the method using values on two height datums. More complex implementations could use multiple height datums. One advantage of using multiple datums is that the additional information can be used to provide an estimate of whether or not the source is homogeneous (Keating, 2009). This would be possible using our implementation; the programme could be run multiple times, with multiple continuation distances. If the estimated index is similar for all runs, then the source is homogeneous.

6. Conclusions

The SLUTH method has been implemented to run on gridded data as a GX in the Geosoft montaj geophysical processing package. The inputs to the GX are a grid of the total field on a measurement datum and the total field on a higher datum, which can be calculated by upward continuation. Also required are the vertical and horizontal derivatives on both datums. The upward continuation and the spatial derivatives can be calculated using the magmap1 GX available in Geosoft Oasis montaj. The outputs from the algorithm are grids of the strike direction, the standard deviation in the strike direction, the index and the depth. The grids are white (dummy or null values) where the dip of the ray plane is greater than 27 degrees. Where the dip is less than 27 the colour is dependent on the strike, strike standard deviation, index and depth, respectively. The depth is also equal to the width of the coloured zone, so a second estimate of the depth can be obtained by looking at the width of the coloured zone. In our synthetic example, we found that the colour of the grid gave an overestimate and the width of the coloured zone a slight underestimate. Of the two estimates, the width appears to be more robust. Nonetheless, variations in colour and widths can be used to map qualitative changes in the depth of features. The depth information obtained from the Saskatoon magnetic data set did not image the depth to the basement well for two reasons. (1) Most of the magnetic sources seem to be deeper than the sediment/basement interface and (2) interference seemed to be a problem. However, it is still possible to extract source parameter information from the data by looking at the images carefully. In the Saskatoon area, zones of weak magnetic response are interpreted as due to basement lows.

Acknowledgements

Richard Smith is grateful to the Industrial Research Chair funded by NSERC, Vale, Xstrata Nickel, QuadraFNX Mining, Wallbridge Mining Company and the Centre for Excellence in Mining Innovation.

Appendix A. Supplementary material

Supplementary data associated with this article can be found in the online version at http://dx.doi.org/10.1016/j.cageo.2012.03.004.

References

Cella, F., Fedi, M., Florio, G., 2009. Toward a full multiscale approach to interpret potential fields. Geophysical Prospecting 57, 543–557. http://dx.doi.org/:10.1111/j.1365-2478.2009.00808.x.

Dean, W.C., 1958. Frequency analysis for gravity and magnetic interpretation. Geophysics 23, 97–127.

Fedi, M., 2007. DEXP: a fast method to determine the depth and the structural index of potential fields sources. Geophysics 72, I1–I11. http://dx.doi.org/:10.1190/1.2399452.

Geological Survey of Canada, 1995. Aeromagnetic total field map, Saskatchewan: NTS 73B/NW, scale 1:100,000. GSC open file number 2955. http://gdr.nrcan.gc.ca/aeromag/index_e.php (accessed 2 September, 2011).

Gerovska, D., Araúzo-Bravo, M.J., Whaler, K., Stavrev, P., Reid, A., 2010. Three-dimensional interpretation of magnetic and gravity anomalies using the finite-difference similarity transform. Geophysics 75, L79–L90. http://dx.doi.org/:10.1190/1.3453765.

Hartman, R.R., Teskey, D.J., Friedherg, J.L., 1971. A system for rapid digital aeromagnetic interpretation. Geophysics 36, 891–918.

Hornby, P., Boschetti, F., Horowitz, F.G., 1999. Analysis of potential field data in the wavelet domain. Geophysical Journal International 137, 175–196.

Keating, P., 2009. Improved use of the local wavenumber in potential-field interpretation. Geophysics 74, L75–L85.

Lahti, I., Karinen, T., 2010. Tilt derivative multiscale edges of magnetic data. The Leading Edge 29, 24–29.

Miller, H.G., Singh, V., 1994. Potential field tilt—A new concept for location of potential field sources. Journal of Applied Geophysics 32, 213–217. http://dx.doi.org/:10.1016/0926-9851(94)90022-1.

Moreau, F., Gibert, D., Holschnider, M., Saracco, G., 1997. Wavelet analysis of potential fields. Inverse Problems 13, 165–178.

Nabighian, M.N., 1972. The analytic signal of two-dimensional magnetic bodies with polygonal cross-section: its properties and use for automated anomaly interpretation. Geophysics 37, 507–517.

Naudy, H., 1971. Automatic determination of depth on aeromagnetic profiles. Geophysics 36, 712–722.

Pasteka, R., Richter, F.P., Karcol, R., Brazda, K., Hajach, M., 2009. Regularized derivatives of potential fields and their role in semi-automated interpretation methods. Geophysical Prospecting 57, 507–516. http://dx.doi.org/:10.1111/j.1365-2478.2008.00780.x.

Reid, A.B., Allsop, J.M., Granser, H., Millet, A.J., Somerton, I.W., 1990. Magnetic interpretation in three dimensions using Euler deconvolution. Geophysics 55, 80–91.

Roest, W.R., Verhoef, J., Pilkington, M., 1992. Magnetic interpretation using the 3-D analytic signal. Geophysics 57, 116–125.

Ruddock, K.A., Slack, H.A., Breiner, S., 1966. Method for determining depth and fall-off rate of subterranean magnetic disturbances utilizing a plurality of magnetometers. US patent, 3263161.

Sailhac, P., Galdeano, A., Gilbert, D., Morcau, F., Delor, C., 2000. Identification of sources of potential fields with the continuous wavelet transform: complex wavelets and application to aeromagnetic profiles in French Guiana. Journal of Geophysical Research 105, 19455–19475.

Sailhac, P., Gibert, D., Boukerbout, H., 2009. The theory of the continuous wavelet transform in the interpretation of potential fields: a review. Geophysical Prospecting 57, 517–525. http://dx.doi.org/:10.1111/j.1365-2478.2009.00794.x.

Salem, A., Smith, R., 2005. Depth and structural index from normalized local wavenumber of 2D magnetic anomalies. Geophysical Prospecting 53, 83–89.

Salem, A., Ravat, D., Smith, R., Ushijima, K., 2005. Interpretation of magnetic data using an enhanced local wavenumber (ELW) method. Geophysics 70, L7–L12.

Salem, A., Williams, S., Fairhead, D., Smith, R., Ravat, D., 2008. Interpretation of Magnetic data using tilt-angle derivatives. Geophysics 73, L1–L10.

Salem, A., Williams, S., Fairhead, J.D., Ravat, D., Smith, R., 2007. Tilt–depth method: a simple depth estimation method using first-order magnetic derivatives. The Leading Edge 26 (December), 1502–1505. http://dx.doi.org/:10.1190/1.2821934.

Salem, A., Williams, S., Samson, E., Fairhead, D., Ravat, D., Blakely, R.J., 2010. Sedimentary basins reconnaissance using the magnetic tilt–depth method. Exploration Geophysics 41, 198–209. http://dx.doi.org/:10.1071/EG10007.

Saskatchewan Geological Survey, 1999. Geological map of Saskatchewan 1:1,000,000 Map. Saskatchewan Industry and Resources, Saskatoon, Saskatchewan. http://www.er.gov.sk.ca/adx/aspx/adxGetMedia.aspx?DocID=5145,4477,3440,3385,5460,2936,Documents&MediaID=13140&Filename=Geological_Map_of_Sask.pdf (accessed 29 August, 2011).

Smith, R.S., Salem, A., 2005. Imaging the depth, structure, and susceptibility from magnetic data: the advanced source parameter imaging method. Geophysics 70, L31–38.

Smith, R.S., Salem, A., Lemieux, J., 2005. An enhanced method for source parameter imaging of magnetic data collected for mineral exploration. Geophysical Prospecting 53, 655–665.

Smith, R.S., Thurston, J.B., Dai, T.-F., MacLeod, I.N., 1998. iSPI™ – the improved source parameter imaging method. Geophysical Prospecting 46, 141–151.

Stavrev, P., and Reid, A., 2007, Degrees of homogeneity of potential fields and structural indices of Euler deconvolution. Geophysics 72, L1–L12. http://dx.doi.org/10.1190/1.2400010.

Stavrev, P., Gerovska, D., Arauzo-Bravo, M.J., 2009. Depth and shape estimates from simultaneous inversion of magnetic fields and their gradient components using differential similarity transforms. Geophysical Prospecting 57, 707–717. http://dx.doi.org/10.1111/j.1365-2478.2008.00765.x.

Thompson, D.T., 1982. EULDPH: a new technique for making computer-assisted depth estimates from magnetic data. Geophysics 47, 31–37.

Thurston, J., Smith, R., 2007. Source location using total-field homogeneity: introducing the SLUTH method for depth estimation. The Leading Edge 26, 1272–1277.

Thurston, J.B., Smith, R.S., 1997. Automatic conversion of magnetic data to depth, dip, and susceptibility contrast using the SPI(TM) method. Geophysics 62, 807–813.

Thurston, J.B., Smith, R.S., Guillon, J.-C., 2002. A multimodel method for depth estimation from magnetic data. Geophysics 67, 555–561.

Ulla, J., Smith, R., Samson, C., Vallée, M., 2010. Automation of the SLUTH method: a novel approach to airborne magnetic data interpretation. Near Surface Geophysics 8, 519–528. http://dx.doi.org/:10.3997/1873-0604.2010033.

Vallee, M.A., Keating, P., Smith, R.S., St-Hilaire, C., 2004. Estimating depth and model type using the continuous wavelet transform of magnetic data. Geophysics 69, 191–199.